Global NEST Journal, Vol 16, No 5, pp 988-997, 2014

SPATIAL AND SEASONAL PATTERNS OF PRECIPITATION IN GREECE: THE TERRAIN SEGMENTATION APPROACH

DEMERTZI K.[1]
PAPAMICHAIL D.[1]
ASCHONITIS V.[2,*]
MILIARESIS G.[3]

[1]*Department of Hydraulics, Soil Science and Agricultural Engineering*
Aristotle University of Thessaloniki, Greece
[2]*Department of Life Sciences and Biotechnology*
University of Ferrara, Italy
[3]*Environmental Conservation & Management*
Faculty of Pure and Applied Sciences
Open University of Cyprus, Cyprus

Received: 06/07/2014
Accepted: 24/09/2014
Available online: 05/12/2014

*to whom all correspondence should be addressed:
e-mail: schvls@unife.it

ABSTRACT

The aim of the study is to investigate the spatial and seasonal variation of precipitation in Greece using multi-temporal data analysis techniques. Mean monthly precipitation grids at ~ 1 km^2 resolution for the period 1950-2000 were used in the analysis. Cross correlation quantified spatio-temporal patterns which are summarized as follows a) the absolute correlations of precipitation versus elevation and longitude are minimized during the winter period, b) the latitude dependency of precipitation presents a seasonal shift where winter precipitation tends to be higher in northern Greece, while summer precipitation tends to be higher in southern Greece. Principal components analysis indicated that the first two components account for the 92.8% of variance in the spatio-temporal variability of precipitation. Cluster analysis segmented the terrain to 27 regions with distinct seasonal variability of precipitation. The majority of irrigated agricultural land (plains of Macedonia, Thessaly and Thrace) belong to clusters which present the lowest values of annual precipitation (<600 mm year^{-1}). The derivation of precipitation signatures for each region of Greece using the proposed terrain segmentation approach can support environmental decision and agricultural planning at a regional (country) scale in relation to water resources management.

Keywords: imagery correlations, principal components, terrain segmentation, environmental decision support, agricultural planning.

1. Introduction

Precipitation is one of the most important hydroclimatic parameters because it regulates the available water for evaporation from soil, transpiration by plants, surface runoff, groundwater recharge and soil moisture increment. These elements are essential for the development of water management planning for agricultural, domestic and industrial-energy uses (McMahon *et al*., 2011; Thenkabail *et al*., 2012; Demertzi *et al*., 2014; Kaffas and Hrissanthou, 2014).

The intra-annual and spatial variability of precipitation for different time scales and sub-regions of Greece have been analyzed using different techniques of multivariate data analysis (Papamichail and Metaxa, 1996; Metaxas *et al*., 1999; Fotiadi *et al*., 1999; Loukas *et al*., 2001; Bartzokas *et al*., 2003; Oikonomou *et al*., 2008; Stathis and Myronidis, 2009; Stathis and Mavromatis, 2009; Nastos and Zerefos, 2010; Feidas *et al*., 2013). On the other hand, a major drawback of such analyses is that a terrain segmentation framework according to the hydroclimatic parameter under study (i.e. precipitation) has not yet been defined for Greece. Thus, sub-regions with distinct seasonal precipitation variability can be defined with the implementation of multi-temporal data analysis techniques.

Representative examples of terrain segmentation techniques have been applied using multi-temporal data of land surface temperature (LST) in an attempt to define sub-regions with different seasonal LST variability, to assess its sensitivity to climatic change and to support environmental analysis (Maeda and Hurskainen, 2014; Miliaresis, 2009; Miliaresis and Partsinevelos, 2010; Miliaresis and Tsatsaris, 2010). In addition Miliaresis (2013, 2014) proposed a method for standardizing multi-temporal LST imagery in order to reveal and describe thermal anomalies using elevation, latitude and longitude dependencies.

The available global grids of monthly precipitation data (Hijmans *et al.*, 2005; Sheffield *et al.*, 2006 etc) stimulate the need for the implementation of terrain segmentation techniques to the hydroclimatic parameters analysis. Such a research effort can quantify the environmental suitability of a certain terrain sub-region according to its distinct seasonal precipitation variability.

The aim of the study is to propose a terrain segmentation framework for the analysis and interpretation of multi-temporal precipitation data. Towards this end, the seasonal variability of precipitation in Greece for the period 1950-2000 will be captured, while the terrain will be segmented to regions with different monthly precipitation signatures. This effort will be valuable in assisting environmental decision support and agricultural planning in relation to water resources management.

2. Data and methods

2.1 Study area and Data

The study area corresponds to Greece (South-East Europe) which is confined between the 34 and 42 parallel North, with a meridional extent from 19 to 28 East and a total area of $\sim 14\times10^4$ km^2. The area is described by Mediterranean climate: mild-cold and rainy winters, relatively warm and dry summers and, generally, extended periods of sunshine throughout most of the year (Hellenic National Meteorological Service, http://www.hnms.gr/hnms/english/climatology/climatology_html). The analysis was based on gridded climatic data which were obtained from the database of Hijmans *et al.*, (2005). The data provide mean monthly values of precipitation at 30 arc-sec spatial resolution (~1×1 km) of the period 1950-2000 (http://www.worldclim.org/). The database also includes a revised version of the GTOPO30 DEM at 30 arc-sec spatial resolution.

2.2 Methods

A set of three statistical methods such as correlation, principal components and k-means cluster analysis were combined in GIS environment for imagery analysis. Correlation analysis and principal component analysis (PCA) were used in order to reveal the temporal and spatial patterns of precipitation. PCA is a linear transformation technique that produces a set of images known as PCAs that are uncorrelated with each other while they are ordered in terms of the amount of variance they explain from the original image set (Maaten and Hinton, 2008). PCAs are computed from the linear combination of eigenvectors and the corresponding pixel values of the initial images (Mather, 2004). PCA has traditionally been used in remote sensing as a means of data compaction since it is common to find that the first 2 or 3 components are able

to explain the majority of the variability in data values, while later components tend to be dominated by noise effects. The rejection of these later components reduces the volume of data with no appreciable loss of information (Siljestrom *et al.,* 1997). Standardized principal components analysis (Eastman and Fulk, 1993) is applied (data per month is centered with mean 0.0 and standard deviation 1.0) and so each image is not weighed according to its variance.

K-means cluster analysis was used to partition the multi-temporal (12-dimensional) imagery of precipitation into K exclusive clusters. It begins by initializing cluster centroids, then assigns each pixel to the cluster whose centroid is nearest, updates the cluster centroids, then repeats the process until the stopping criteria are satisfied (Mather, 2004). The analysis uses Euclidian distance for calculating the distances between pixels and cluster centroids. The underlying idea of cluster analysis is that the cluster centroids represent the mean expression of the derived clusters. Thus, clustering of the multi-temporal data sets is expected to define groups of pixels with a rather common centroid curve that expresses their average monthly variability (Miliaresis, 2009). Elevation, latitude and longitude statistics per cluster are computed in order to assist interpretation. Finally the clusters are interpreted according to their centroid and their spatial arrangement (Miliaresis, 2014). In the current implementation of the method, small clusters with area extent (occurrence) less than 0.001% were eliminated by merging them with larger clusters which are closest to their centroids, while the stopping criterion was defined as the percentage of the migrating pixels during a specific iteration (if it was less than 0.001% of the entire number of image pixels, the clustering was terminated). The maximum number of clusters is defined by a trial and error procedure while the maximum number of iterations is set equal to 300.

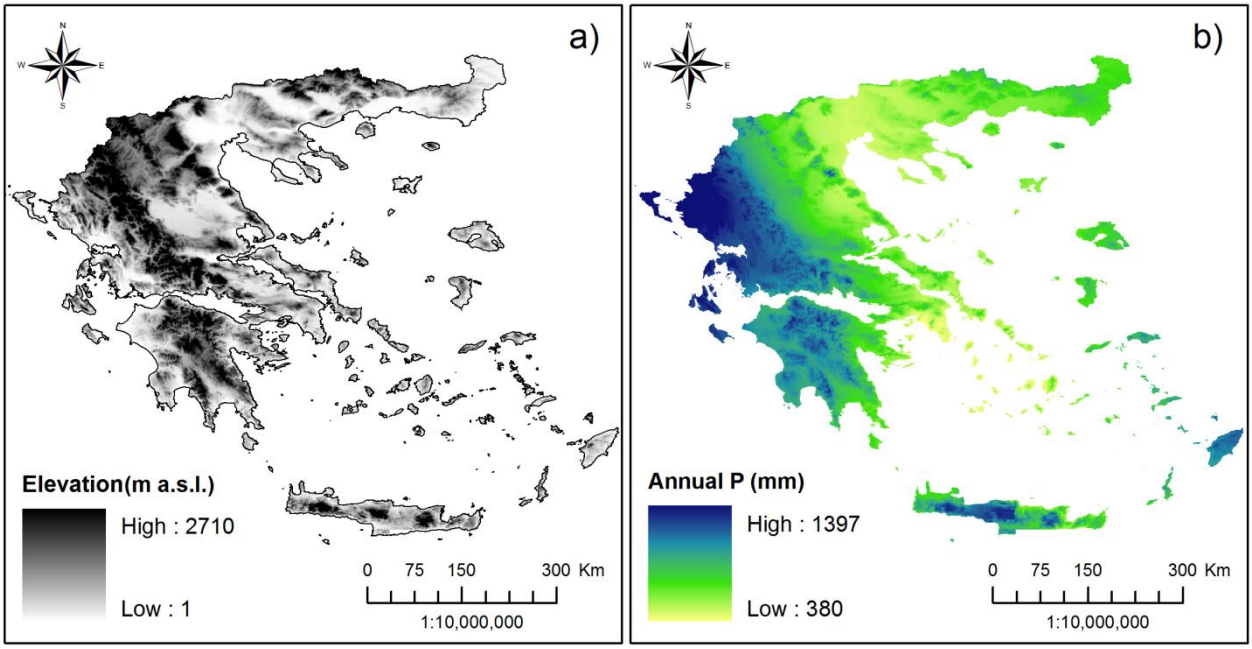

Figure 1. Maps of a) elevation *H* (meters above sea level), b) mean annual precipitation *P* (mm year^{-1}) for the period 1950-2000.

3. Results and Discussion

3.1 Spatial variation of annual precipitation

The 30 arc-sec resolution maps of elevation *H* and mean annual precipitation *P* are given in Figures 1a and 1b, while their frequency distributions are given in Figures 2a and b. The precipitation map (Figure 1b) indicates that the highest annual *P* values are observed in western Greece due to the strong effect of the Pindos mountain range which constitutes a physical obstacle in the movement of vapour masses originated from the southern Alpine system of northern Italy. Apart from the high elevation regions (above 1000 m) in western Greece, other regions with high precipitation are observed in Crete and Rhodes islands located in Southern Greece where in the first case the White, Psiloritis and Dikti mountains (in Grete) and in the second case the Babadag, Uyluk and Bey mountains (western Taurus mountains range in Turkey near Rhodes) block the incoming vapour masses from the Libyan Sea leading to precipitation increase. The mean annual value of precipitation over Greece was estimated at 699 mm.

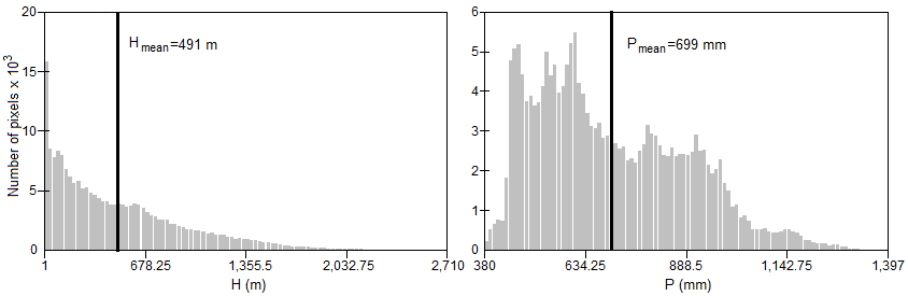

Figure 2. Frequency analysis of the spatial variation of a) elevation *H*, b) mean annual precipitation *P* for the period 1950-2000.

3.2 Spatial and seasonal variation of monthly precipitation

The correlation matrix of the mean monthly precipitation *P* versus elevation *H*, latitude *Lat* and longitude *Lon* is quantified in Table 2. Figure 3 indicates a positive correlation between *P* and *H* where the effects of elevation are minimized during winter. The correlation between *P* and *Lat* is positive during the warm-dry season and negative during the cold-wet season (October-March) (Figure 3) indicating a seasonal shift of the system. Thus, *P* during winter tends to be higher in northern Greece while during summer tends to be higher in southern Greece. The correlation between *P* and *Lon* is always negative indicating a tendency for higher *P* in western Greece while its effects are minimized during winter (Figure 3).

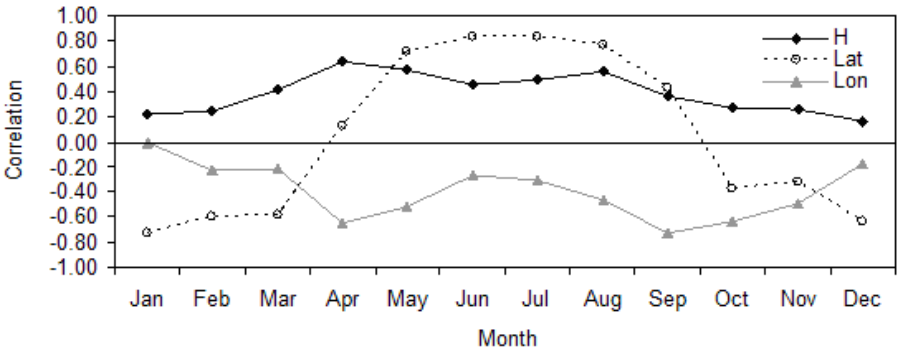

Figure 3. Correlation of mean monthly *P* versus *Lat*, *Lon* and *H*.

Table 2. Cross correlation matrix between *H*, *Lat*, *Lon* and the multi-temporal monthly *P* images.

	H	Lat	Lon	Jan	Feb	Mar	Apr	May	Jun	Jul	Aug	Sep	Oct	Nov	Dec
H	1														
Lat	0.03	1													
Lon	-0.30	-0.14	1												
Jan	0.22	-0.72	0.00	1											
Feb	0.24	-0.60	-0.23	0.93	1										
Mar	0.41	-0.58	-0.21	0.93	0.96	1									
Apr	0.64	0.12	-0.65	0.39	0.58	0.63	1								
May	0.57	0.71	-0.51	-0.29	-0.14	-0.03	0.67	1							
Jun	0.45	0.83	-0.26	-0.49	-0.37	-0.26	0.45	0.90	1						
Jul	0.49	0.83	-0.31	-0.52	-0.42	-0.30	0.41	0.93	0.96	1					
Aug	0.55	0.76	-0.46	-0.40	-0.27	-0.16	0.54	0.96	0.89	0.95	1				
Sep	0.36	0.42	-0.73	0.12	0.35	0.35	0.85	0.76	0.54	0.53	0.67	1			
Oct	0.26	-0.37	-0.64	0.71	0.83	0.82	0.75	0.15	-0.14	-0.16	0.02	0.66	1		
Nov	0.25	-0.32	-0.49	0.76	0.87	0.81	0.70	0.09	-0.18	-0.19	0.00	0.62	0.92	1	
Dec	0.17	-0.63	-0.17	0.96	0.96	0.92	0.50	-0.22	-0.45	-0.50	-0.35	0.27	0.81	0.88	1

In order to further interpret the monthly inter-correlations observed in Table 2, principal components analysis (PCA) was implemented and the corresponding eigenvalues and eigenvectors are presented in Table 3. According to the eigenvalues (Table 3), the first two principal components (PC-1 and PC-2) account for the 92.8 % of the total variance observed in the 12 monthly *P* images. The PC-1 map (Figure 4a) is composed by linear combinations of monthly *P* images that amplify the difference between the periods of May-August (negative signs) versus October-April (positive signs) (Table 3). The PC-1 is spatially maximised in the western and south-eastern Greece. For PC-2, the linear combinations of monthly *P* images amplify the difference between the periods of October-March and April-September. The difference between these two periods is spatially maximised in the north-western Greece and in the mountainous regions of Rhodope while it is minimized in the lowland regions of southern Greece and in the islands of Aegean sea.

Table 3. Eigenvalues and eigenvectors for the PCs of the multi-temporal *P* monthly images.

P	Principal Components (PCs)											
Eigenvectors	1	2	3	4	5	6	7	8	9	10	11	12
Jan	0.38	-0.07	-0.41	0.28	0.03	-0.26	0.02	-0.33	-0.03	0.12	0.51	-0.40
Feb	0.39	0.01	-0.16	-0.12	-0.11	0.20	-0.44	0.33	-0.67	0.06	-0.05	0.01
Mar	0.38	0.05	-0.41	-0.13	0.36	-0.15	-0.20	0.28	0.51	-0.26	-0.22	0.16
Apr	0.23	0.36	-0.06	-0.46	-0.06	0.60	0.31	-0.06	0.16	0.01	0.34	-0.03
May	-0.07	0.44	-0.12	0.03	0.14	0.08	-0.11	-0.56	-0.22	-0.42	-0.40	-0.22
Jun	-0.17	0.39	-0.28	-0.26	-0.51	-0.41	0.12	0.24	0.06	0.21	-0.20	-0.29
Jul	-0.18	0.39	-0.22	0.22	0.01	-0.21	0.18	0.12	-0.25	-0.26	0.37	0.60
Aug	-0.12	0.42	-0.06	0.46	0.38	0.26	-0.03	0.21	0.06	0.56	-0.12	-0.11
Sep	0.14	0.39	0.48	-0.04	-0.14	-0.20	-0.60	-0.15	0.25	0.08	0.27	0.10
Oct	0.35	0.15	0.39	-0.26	0.43	-0.43	0.41	0.01	-0.27	0.15	-0.10	-0.01
Nov	0.36	0.13	0.32	0.50	-0.31	0.09	0.25	0.32	0.09	-0.40	-0.09	-0.23
Dec	0.39	-0.03	-0.10	0.17	-0.35	0.04	0.15	-0.39	0.08	0.35	-0.36	0.50
Eigenvalues	6.26	4.88	0.44	0.14	0.10	0.07	0.05	0.04	0.01	0.01	0.01	0.00
Variance %	52.13	40.66	3.63	1.17	0.84	0.56	0.46	0.30	0.11	0.07	0.06	0.02

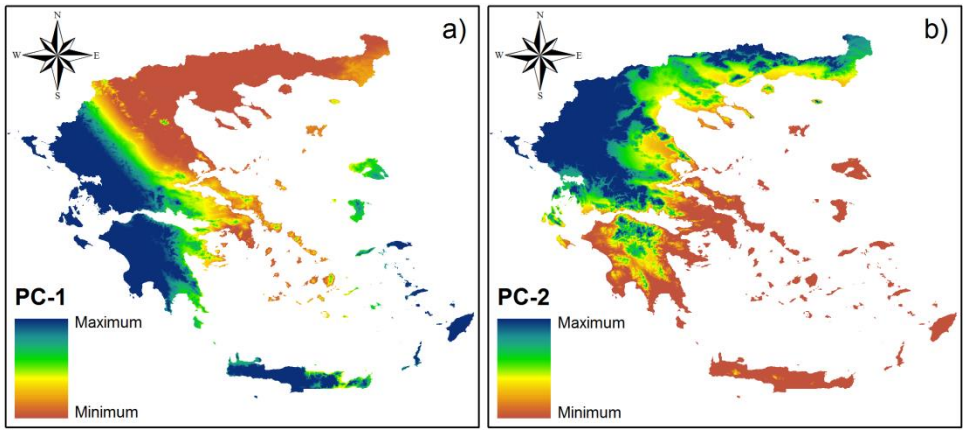

Figure 4. The first two principal components a) PC-1 and b) PC-2, that account for the 92.8% of the *P* variance according to Table 3.

3.3 Terrain segmentation based on the spatial and seasonal variation of monthly precipitation

Cluster analysis provided 27 precipitation clusters where their spatial distribution is given in Figure 5. Their centroids (latitude, longitude), their percent area extent, mean elevation and the variation of monthly precipitation are given in Table 4. Considering the whole Greece, *P* is minimized during August and maximized during December, while the 27% of precipitation is observed during April to September (warm-dry period) and the 73% during the October to March (cold-wet period) (Table 4). Clusters which present significant deviations from the aforementioned general trends or other particular characteristics are the following:

- Cluster 2 (with the greatest area extent) presents a) the lowest value of annual precipitation and b) the highest percentage of precipitation (41.6%) during the April-September period.
- Cluster 2 together with Cluster 1 and 5 cover approximately 39% of Greece and present the lowest values of annual precipitation (<600 mm year^{-1}). It is indicative that these clusters include the plains of Macedonia, Thessaly and Thrace which host the majority of irrigated agricultural land in Greece.
- Cluster 24 (Rhodes island) presents α) 25% higher annual precipitation from the mean precipitation in Greece and b) the lowest percentage of precipitation (8%) during the April-September period.
- Clusters 10, 11, 12, 13 and 20 (north-western Greece) are of particular interest because they present the highest values of annual precipitation exceeding 1000 m year^{-1}.
- Clusters 3, 4, 6, 7, 9, 18, 22 and 27 cover the regions of the highest elevation (>900 m) providing significant information about the precipitation patterns in the mountainous areas.
- Clusters 1 and 3 are of particular interest because they present high geographical dispersion.

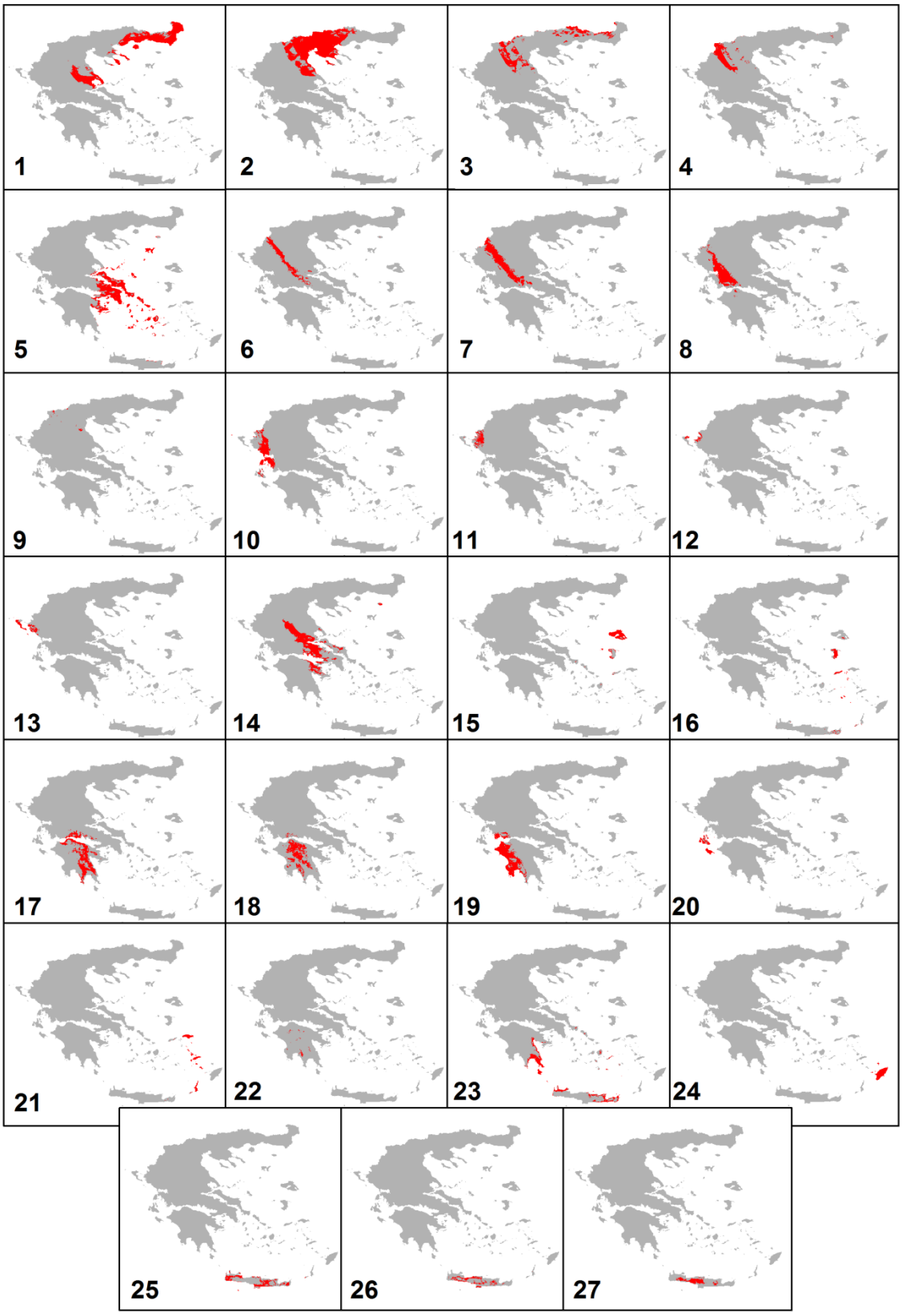

Figure 5. The spatial distribution of the 27 precipitation clusters.

Table 4. Centroids coordinates, percent area extent, mean elevation *H*, monthly and annual precipitation *P* of each cluster.

Cluster	Centroid		Area	*H*	*P* (mm)												
	Lat	*Lon*	%	(m)	Jan	Feb	Mar	Apr	May	Jun	Jul	Aug	Sep	Oct	Nov	Dec	Annual
1	40.56	24.49	11.50	225	66	53	54	43	44	39	24	16	30	54	70	78	571
2	40.67	22.89	17.88	321	45	39	44	38	50	38	29	23	29	46	59	56	494
3	40.69	22.95	6.06	922	63	53	58	53	62	50	37	30	36	59	74	72	647
4	40.31	21.45	3.23	946	75	63	65	63	68	44	37	33	44	80	91	85	749
5	38.15	23.91	9.45	209	76	60	57	32	23	13	7	7	18	56	67	87	501
6	39.50	21.64	2.70	924	99	83	77	68	62	43	31	25	43	88	101	114	835
7	39.39	21.45	4.98	1319	117	96	88	75	66	45	34	30	47	95	120	130	942
8	38.98	21.34	4.37	588	126	112	88	68	52	34	21	18	46	104	134	151	955
9	40.43	21.98	0.16	1979	97	78	85	76	78	59	46	43	44	74	99	101	879
10	39.17	20.79	3.32	447	140	123	94	70	52	29	19	20	55	119	160	169	1048
11	39.68	20.50	1.05	506	157	141	105	81	62	33	22	26	65	128	183	189	1192
12	39.74	20.21	0.36	367	170	156	112	82	58	27	18	25	71	138	202	209	1268
13	39.49	20.17	0.83	159	150	138	98	70	47	19	12	19	69	135	188	186	1131
14	38.76	22.62	7.09	403	89	75	68	52	41	31	17	13	30	73	78	108	674
15	39.01	26.16	1.45	219	116	92	67	40	26	12	6	5	16	37	85	130	632
16	37.57	26.13	0.91	366	132	98	75	36	21	8	4	2	13	46	81	138	656
17	37.66	22.41	4.97	564	114	91	75	53	34	20	12	10	28	81	111	135	763
18	37.68	22.13	3.87	1021	134	105	87	62	41	26	17	15	33	90	125	152	886
19	37.58	21.71	5.23	248	122	96	75	50	28	12	7	8	32	98	133	150	813
20	38.08	20.66	0.81	250	149	111	90	53	29	11	8	11	44	129	160	184	980
21	36.85	26.99	0.99	282	168	108	82	35	22	4	1	1	13	53	92	162	742
22	37.30	22.24	0.22	1633	154	116	101	68	45	27	19	17	33	92	129	163	965
23	36.19	23.97	3.08	212	111	77	68	34	17	5	3	3	16	68	87	114	602
24	36.20	27.94	1.08	216	216	101	94	29	23	3	2	1	13	69	121	207	877
25	35.23	24.79	1.91	379	149	103	89	37	18	6	2	2	15	78	88	135	723
26	35.24	24.69	1.24	541	176	125	109	43	22	9	4	2	18	92	98	156	854
27	35.24	24.64	1.24	1003	200	139	125	51	28	13	6	4	20	98	108	175	968
Total Greece					94	75	68	49	43	29	20	17	32	72	92	108	699

4. Conclusions

Cross correlation and principal components quantified the spatio-temporal patterns of precipitation revealing seasonal, latitudinal, longitudinal and elevation dependencies. The most significant findings were that a) the absolute correlations of precipitation versus elevation and longitude are minimized during the winter period, b) the latitude dependency of precipitation presents a seasonal shift where winter precipitation tends to be higher in northern Greece while summer precipitation tends to be higher in southern Greece and c) the first two principal components account for the 92.8% of variance in the spatio-temporal variability of precipitation in Greece

Cluster analysis segmented the terrain to 27 regions with distinct seasonal variability of precipitation, while the clusters which cover the majority of irrigated agricultural land (approximately 39% of Greece) present the lowest values of annual precipitation (<600 mm year^{-1}).

The terrain segmentation according to the mean monthly values of *P* for a 50 year period is a valuable tool for supporting environmental-agricultural decision support and risk assessment related to water resources

management. Future attempts may also focus on the use of cluster analysis to climate change studies such as a) to assess the monthly precipitation changes within each cluster by integrating monthly *P* data sets of the fore-coming years or to b) to use the data sets of the fore-coming years in order to recompute clusters in an attempt to evaluate any trends in the centroid change between two periods.

Supplementary Material

The supplementary material includes a polygon shapefile projected in WGS84 ellipsoid with the 27 clusters of Table 4. Each polygon contains the identity cluster number of *P* from Table 4.The file can be downloaded by the following source:

https://www.researchgate.net/publication/263660546

References

Bartzokas A., Lolis C.J. and Metaxas D.A. (2003), A study of the intra-annual variation and the spatial distribution of precipitation amount and duration over Greece on 10 day basis, *International Journal of Climatology*, **23**, 207-222.

Demertzi K.A., Papamichail D.M., Georgiou P.E., Karamouzis D.N. and Aschonitis V.G. (2014), Assessment of rural and highly seasonal tourist activity plus drought effects on reservoir operation in a semi-arid region of Greece using the WEAP model, *Water International,* **39**, 23-34.

Eastman J.R. and Fulk M. (1993), Long sequence time series evaluation using standardized principal components, *Photogrammetric Engineering & Remote Sensing,* **59**, 1307-1312.

Feidas H., Karagiannidis A., Keppas S., Vaitis M., Kontos T., Zanis P., Melas D. and Anadranistakis E. (2014), Modeling and mapping temperature and precipitation climate data in Greece using topographical and geographical parameters, *Theoretical and Applied Climatology*, (in press), doi:10.1007/s00704-013-1052-4.

Fotiadi A.K., Metaxas D.A. and Bartzokas A. (1999), A statistical study of precipitation in NW Greece, *International Journal of Climatology*, **19**, 1221-1232.

Hijmans R.J., Cameron S.E., Parra J.L., Jones P.G. and Jarvis A. (2005), Very high resolution interpolated climate surfaces for global land areas, *International Journal of Climatology,* **25**, 1965-1978.

Kaffas K. and Hrissanthou V. (2014), Application of a continuous rainfall-runoff model to the basin of Kosynthos river using the hydrologic software HEC-HMS, *Global Nest Journal*, **16**, 188-203.

Loukas A., Vasiliades L., Dalezios N.R. and Domenikiotis C. (2001), Rainfal-frequency mapping for Greece, *Physics and Chemistry of the Earth Part. B,* **26**, 669-674.

Maaten L. and Hinton G. (2008), Visualizing High-Dimensional Data Using t-SNE, *Journal of Machine Learning Research,* **9**, 2579-2605.

Mather P.M. (2004), Computer processing of remotely-sensed images (3rd edition), New York: John Wiley and Sons, 442 p.

Maeda E. and Hurskainen P. (2014), Spatiotemporal characterization of land surface temperature in Mount Kilimanjaro using satellite data, *Theoretical and Applied Climatology*, (in press), doi: 10.1007/s00704-013-1082-y

Miliaresis G. (2009), Regional thermal and terrain modeling of the Afar Depression from multi-temporal night LST data, *International Journal of Remote Sensing,* **30**, 2429-2446.

Miliaresis G. and Partsinevelos P. (2010), Terrain Segmentation of Egypt from Multi-temporal Night LST Imagery and Elevation Data, *Remote Sensing,* **2**, 2083-2096.

Miliaresis G. and Tsatsaris A. (2010), Thermal terrain modeling of spatial objects, a tool for environmental and climatic change assessment, *Environmental Monitoring & Assessment,* **164**, 561-572.

Miliaresis G. (2013), Thermal_anomaly mapping from night MODIS imagery of USA, a tool for environmental assessment. *Environmental Monitoring & Assessment,* **185**, 1601-1612.

Miliaresis G. (2014), Spatiotemporal patterns of land surface temperature of Antarctica from MODIS Monthly LST data (MYD11C3), *Journal of Spatial Sciences,* **59**, 157-166.

McMahon T.A., Peel M.C., Pegram G.G.S. and Smith I.N. (2011), A simple methodology for estimating mean and variability of annual runoff and reservoir yield under present and future climates, *Journal of Hydrometeorology,* **12**, 135-146.

Metaxas D.A., Philandras C.M., Nastos P.T. and Repapis C.C. (1999), Variability of precipitation pattern in Greece during the year, *Fresenius Environmental Bulletin*, **8**, 1-6.

Nastos P.T. and Zerefos C.S. (2010), Cyclic modes of the intra-annual variability of precipitation in Greece, *Advances in Geosciences*, **25**, 45-50.

Oikonomou C., Flocas H.A., Hatzaki M., Asimakopoulos D.N. and Giannakopoulos C. (2008), Future changes in the occurrence of extreme precipitation events in Eastern Mediterranean, *Global Nest Journal*, **10**, 255-262.

Papamichail D.M. and Metaxa I.G. (1996), Geostatistical analysis of spatial variability of rainfall and optimal design of a rain gauge network, *Water Resources Management*, **10**, 107-127.

Sheffield J., Goteti G. and Wood E.F. (2006), Development of a 50-yr high-resolution global dataset of meteorological forcings for land surface modeling, *Journal of Climate*, **19**, 3088-3111.

Siljestrom P.A., Moreno A., Vikgren G. and Caceres L.M. (1997), The application of selective principal components analysis to a Thematic Mapper image for the recognition of geomorphologic features configuration, *International Journal of Remote Sensing,* **18**, 3843-3852.

Stathis D. and Myronidis D. (2009), Principal component analysis of precipitation in Thessaly region (central Greece), *Global Nest Journal*, **11**, 467-476.

Stathis D. and Mavromatis T. (2009), Characteristics of precipitation in Thessaloniki area, North Greece, *Fresenius Environmental Bulletin*, **18**, 1270-1275.

Thenkabail P.S., Knox J.W., Ozdogan M., Gumma M.K., Congalton R.G., Wu Z., Milesi C., Finkral A., Marshall M., Mariotto I., You S., Giri C.P. and Nagler P.L. (2012), Assessing future risks to agricultural productivity, water resources and food security-how can remote sensing help?, *Photogrammetric Engineering & Remote Sensing,* **78**, 773-782.